

The Lack of a QBO-MJO Connection in Climate Models with a Nudged Stratosphere

Zane K. Martin¹, Isla R. Simpson², Pu Lin³, Clara Orbe⁴, Qi Tang⁵, Julie M. Caron², Chih-Chieh Chen², Hyemi Kim^{6,7}, L. Ruby Leung⁸, Jadwiga H. Richter², Shaocheng Xie⁵

¹Department of Atmospheric Science, Colorado State University, Fort Collins, CO

²Climate and Global Dynamics Laboratory, National Center for Atmospheric Research, Boulder, CO

³Program in Atmospheric and Oceanic Science, Princeton University, Princeton, NJ

⁴NASA Goddard Institute for Space Studies, New York, NY

⁵Lawrence Livermore National Laboratory, Livermore, CA

⁶Department of Science Education, Ewha Womans University, Seoul, Republic of Korea

⁷School of Marine and Atmospheric Sciences, Stony Brook University, Stony Brook, NY

⁸Atmospheric Sciences and Global Change, Pacific Northwest National Laboratory, Richland, WA

Key Points:

- The link between the quasi-biennial oscillation (QBO) and Madden-Julian oscillation (MJO) is explored in four climate models with nudged stratospheric winds and free-evolving tropospheres.
- No model shows as strong of a QBO-MJO connection as in observations.
- Model biases in cloud-radiative feedbacks and MJO vertical velocity are diagnosed, but neither conclusively explains the lack of a QBO-MJO connection.

Corresponding author: Clara Orbe, clara.orbe@nasa.gov

Abstract

The observed stratospheric quasi-biennial oscillation (QBO) and the tropospheric Madden-Julian oscillation (MJO) are strongly connected in boreal winter, with stronger MJO activity when lower-stratospheric winds are easterly. However, the current generation of climate models with internally generated representations of the QBO and MJO do not simulate the observed QBO-MJO connection, for reasons that remain unclear. This study builds on prior work exploring the QBO-MJO link in climate models whose stratospheric winds are relaxed towards reanalysis, reducing stratospheric biases in the model and imposing a realistic QBO. A series of ensemble experiments are performed using four state-of-the-art climate models capable of representing the MJO over the period 1980-2015, each with similar nudging in the stratosphere. In these four models, nudging leads to a good representation of QBO wind and temperature signals, however no model simulates the observed QBO-MJO relationship. Biases in MJO vertical structure and cloud-radiative feedbacks are investigated, but no conclusive model bias or mechanism is identified that explains the lack of a QBO-MJO connection.

Plain Language Summary

Observations show a strong link between the stratospheric quasi-biennial oscillation (QBO) — the alternation of tropical stratospheric zonal winds between easterly and westerly phases — and the Madden-Julian oscillation (MJO), an eastward propagating phenomenon in the tropical troposphere in which the circulation and convection are coupled. Stronger MJO activity is observed when lower-stratospheric winds are easterly. This coupling is intriguing for many reasons, but most practically because it suggests that the stratosphere can potentially enhance surface weather and inform subseasonal climate prediction. However, current climate models do not show this observed connection. One reason may be related to biases in how models simulate stratospheric winds, which can be corrected for in an artificial way by relaxing the model simulated winds to better match observationally-constrained data sets. One recent study, however, showed that correcting for this bias using this approach in one climate model still fails to produce credible QBO-MJO coupling. Here we expand that analysis to include four climate models and find that no model produces a robust QBO-MJO relationship like that seen in observations. Our results show that properly representing the QBO winds and temperatures via nudging is therefore not sufficient for reproducing the observed relationship. Furthermore, while biases in how models represent cloud processes may still be a likely culprit, any definitive model bias or missing mechanism remains elusive.

1 Introduction

The quasi-biennial oscillation (QBO; Ebdon (1960); Reed et al. (1961); Baldwin et al. (2001) - a descending, ~ 28 month reversal in the tropical stratospheric zonal wind - is the most significant mode of interannual variability in the tropical stratosphere. While QBO signals are strongest in the tropical stratosphere, through teleconnections, the QBO modulates climate processes outside the tropics and below the stratosphere (Holton and Tan (1980); Camargo and Sobel (2010); Garfinkel and Hartmann (2011); Gray et al. (2018); Anstey et al. (2022)). In particular, a strong connection has recently been observed between the QBO and the Madden-Julian oscillation (MJO; Madden and Julian (1971, 1972)), a subseasonal, eastward propagating envelope with strong coupling of tropical convection and circulation. During boreal winter, MJO activity and strength is significantly enhanced when the QBO is in the easterly phase relative to the westerly phase (Yoo and Son (2016); Son et al. (2017); Martin, Son, et al. (2021)). This QBO-MJO connection modulates MJO predictability and its teleconnections (Marshall et al. (2017); J. Wang et al. (2018); Lim et al. (2019); S. Wang et al. (2019); H. Kim et al. (2019); Feng and Lin (2019); Toms et al. (2020); Mayer and Barnes (2020)). Yet despite these far-reaching impacts,

71 the QBO-MJO connection remains theoretically difficult to explain (Martin, Son, et al.
72 (2021)).

73 Challenges in understanding the physics behind the QBO-MJO connection are in
74 large part hampered by the inability of climate models to capture the connection. While
75 convection-permitting models (Martin et al. (2019); Back et al. (2020)) and subseasonal
76 forecast models (Abhik and Hendon (2019); Martin et al. (2020)) have shown some in-
77 dication of a QBO-MJO link, model signals in both frameworks are weaker-than-observed
78 and difficult to confidently detect or interpret. Free-running global climate models (GCMs)
79 present an alternative framework in which to examine this problem, which is attractive
80 given that many GCMs are now capable of internally simulating both a QBO and an MJO
81 (e.g., Richter et al. (2020); Ahn et al. (2020); Orbe, Van Roekel, et al. (2020); H. Kim
82 et al. (2020)). However, GCMs have repeatedly failed to show any QBO-MJO link (Lee
83 and Klingaman (2018); H. Kim et al. (2020); Lim and Son (2020); Martin, Orbe, et al.
84 (2021)).

85 A frequent hypothesis for why climate models do not capture a QBO-MJO con-
86 nection are biases in the model stratosphere, in particular the QBO representation in
87 the lower stratosphere and the tropical tropopause layer (TTL) (Martin et al. (2019);
88 Lee and Klingaman (2018); H. Kim et al. (2020); Lim and Son (2020); Martin, Son, et
89 al. (2021)). Most state-of-the-art climate models show weaker-than-observed QBO vari-
90 ability in the TTL, in particular in QBO temperature signals. These biases might be im-
91 portant, as QBO temperature anomalies and their effect on upper tropospheric static
92 stability are a proposed mechanism for the QBO-MJO connection (Martin, Son, et al.
93 (2021)). A straightforward way to test the hypothesis that stratospheric biases in mod-
94 els explain the lack of a QBO-MJO link is to impose the stratosphere in the model by
95 “nudging” (e.g., Ferranti et al. (1990); Jeuken et al. (1996); Douville (2009); Hitchcock
96 and Simpson (2014)). This is done by adding artificial tendency terms that relax the model
97 towards a target profile such as reanalysis (e.g., Jeuken et al. (1996)). In the context of
98 the QBO-MJO link, (Martin, Orbe, et al., 2021) (herein M21) carried out a nudged cli-
99 mate model experiment in which the global stratospheric meridional and zonal winds were
100 relaxed towards reanalysis while the troposphere was not nudged. M21 showed that while
101 QBO winds and temperatures were captured successfully in the nudged model, no QBO-
102 MJO link was evident across an ensemble of simulations.

103 Here, we extend the work in M21 by repeating a similar stratospheric nudging ex-
104 periment across four state-of-the-art climate models, each with several ensemble mem-
105 bers run from 1980 to 2014. The use of multiple models allows us to explore the degree
106 to which the findings in M21 were model specific, and to increase confidence that the re-
107 sults of that study were robust. Further, they allow us to explore whether models share
108 any common biases important to the QBO-MJO link.

109 In Section 2, we present more details regarding the four GCMs and the stratospheric
110 nudging experimental design, as well as other datasets and methodology. Section 3 di-
111 agnoses the nudged models’ representation of the QBO (Sect. 3.1), the MJO (Sect. 3.2)
112 and the QBO-MJO connection (Sect. 3.3). Section 4 summarizes our findings.

113 2 Data and Methods

114 2.1 Climate Models and Nudging Experimental Design

115 Simulations were conducted using four atmosphere-ocean coupled climate models:
116 the Community Earth System Model, version 2 (referred to here as CESM, Danabasoglu
117 et al. (2020)); the Energy Exascale Earth System Model version 1 (referred to here as
118 E3SM, Golaz et al. (2019)); the Geophysical Fluid Dynamics Laboratory CM4 (referred
119 to here as GFDL, Held et al. (2019)); and the NASA Goddard Institute for Space Stud-
120 ies Model E2.1-G (referred to here as GISS, Kelley et al. (2020)).

121 In each of the four models, a 3-member ensemble of simulations was conducted over
 122 the historical period from January 1, 1980 to December, 31, 2014 with the CMIP6 his-
 123 torical forcings (Eyring et al. (2016)). In each simulation, the model stratospheric zonal
 124 and meridional wind were nudged towards time-varying reanalysis fields over the same
 125 time period. CESM, GFDL, and GISS were nudged to NASA’s Modern-Era Retrospec-
 126 tive Analysis for Research and Applications 2 (MERRA-2; Gelaro et al. (2017)) reanal-
 127 ysis, while E3SM was nudged to ERA-Interim reanalysis (ERA-I; Dee et al. (2011)) due
 128 to data availability for nudging in that model. The nudging relaxation timescale in all
 129 models was set to 12 hours, and nudging was only implemented above 150 hPa. To smooth
 130 the transition from the nudged stratosphere to the non-nudged troposphere, the nudg-
 131 ing timescales varied linearly from 150 to 100 hPa, with strict nudging above 100 hPa,
 132 and no nudging below 150 hPa. Nudging was implemented globally at all latitudes and
 133 was identically implemented in each ensemble member of a given model.

134 Nudging can be applied in several ways (see M21); we explore two strategies here.
 135 One option is to implement nudging such that the full 3-D spatial structure of the model
 136 is nudged towards the 3-D reanalysis at each grid point (“grid-point nudging”). An al-
 137 ternative approach is to nudge only the zonal-mean of model variables to match the zonal-
 138 mean of reanalysis (“zonal-mean nudging”, Simpson et al. (2011); Hitchcock and Simp-
 139 son (2014)). Note the latter case is not the same as nudging the model at each grid point
 140 to the zonal mean: zonal asymmetries are allowed to exist in the zonal-mean nudged mod-
 141 els. M21 found their overall results were insensitive to which nudging implementation
 142 was used, and zonal-mean nudging can be technically difficult to implement in certain
 143 model frameworks, especially those with unstructured grids. As such, both approaches
 144 were explored in this study. The CESM and GISS models used zonal-mean nudging, whereas
 145 the GFDL and E3SM models used grid-point nudging.

146 2.2 Other Datasets and Methodology

147 Model performance is compared to observational and reanalysis products. In ad-
 148 dition to MERRA-2 reanalysis, observed outgoing long-wave radiation (OLR) from the
 149 NOAA Interpolated OLR dataset (Liebmann and Smith (1996)), observed precipitation
 150 from the Tropical Rainfall Measuring Mission (TRMM; Liu et al. (2012) version 7 Level
 151 3 daily TRMM-3B42 data), and some additional meteorological variables from ERA-5
 152 reanalysis (Hersbach et al. (2020)) are used.

153 MJO indices are a common and useful way to summarize MJO characteristics. We
 154 use the Real-time Multivariate MJO index (RMM; Wheeler and Hendon (2004)) here.
 155 RMM is based on an empirical orthogonal function (EOF) analysis of tropical OLR and
 156 zonal winds. The observed MJO index used is available from the Australian Bureau of
 157 Meteorology (see Data Availability), while for the model simulations the RMM index
 158 is calculated following Wheeler and Hendon (2004), except that the model data are pro-
 159 jected onto the observed rather than the model EOFs. This facilitates a fair compari-
 160 son across models and between models and observations. The OLR-based MJO Index
 161 (OMI; Kiladis et al. (2014)) was also explored, but as overall results discussed below were
 162 not sensitive to the choice of index (as was also found in M21) we present only results
 163 using RMM here.

164 We define the QBO phase using the monthly 50 hPa tropical zonal winds (e.g., Yoo
 165 and Son (2016); Son et al. (2017); Martin, Son, et al. (2021)), averaged zonally and from
 166 10°N to 10°S (U50). QBO easterly months are defined when U50 is less than the mean
 167 minus half a standard deviation (QBOE) and QBO westerly months are defined when
 168 U50 is greater than the mean plus half a standard deviation (QBOW).

169 We further diagnose the representation of the stratospheric transformed Eulerian
 170 mean (TEM) vertical velocity. Due to data availability, ERA5 reanalysis was used to cal-

171 culate TEM quantities for comparison to the four model simulations. Model TEM quan-
 172 tities were calculated following the DynVarMIP protocol (Gerber and Manzini (2016)).

173 3 Results

174 3.1 Nudged QBO and Stratospheric Representation

175 Nudging the model stratosphere leads to an accurate representation of the QBO
 176 signal across all four models, consistent with the strict nudging timescales and with re-
 177 sults in M21. Figure 1 shows the time-series of tropical-mean zonal-mean wind in MERRA-
 178 2 reanalysis and the first ensemble member of each model: the descending alternating
 179 easterly and westerly phases of the QBO are robustly captured in all models with nudg-
 180 ing and match the reanalysis. Furthermore, despite the fact that temperature is not nudged
 181 in any model, QBO temperature signals are represented with fidelity down into the up-
 182 per troposphere. For example, composites of QBO differences (QBOE minus QBOW)
 183 in temperature in reanalysis and each model shown in the right panels of Figure 1 in-
 184 dicate that the structure and magnitude of these temperature signals in the upper tro-
 185 posphere and lower stratosphere are successfully represented in the models with nudg-
 186 ing. Overall, little variation in the QBO temperature signals is evident across models,
 187 again consistent with the fact that the zonal mean winds in all models is strictly nudged
 188 towards reanalysis and temperatures adapt to be in balance with these nudged winds.

189 The time-series of U50 further indicates how closely the models match the reanal-
 190 ysis of the zonal winds. Figure 2a shows the time series of U50, and the CESM, GFDL,
 191 and GISS values are nearly indistinguishable from the target reanalysis. Slight differ-
 192 ences are evident in E3SM, due to the different reanalysis used as a target in this model
 193 (ERA-I); we confirmed that E3SM closely matches the ERA-I U50 (not shown). The tem-
 194 perature at 100 hPa averaged over the tropics (10°S to 10°N) is also shown in Figure 2b;
 195 here there is more variability both between models and within the ensemble. A domi-
 196 nant mode of variability in addition to the QBO in the 100 hPa temperature is the an-
 197 nual cycle, which all models capture to varying degrees. The GFDL and GISS models
 198 tend to be biased warm – the GISS model especially so in winter, whereas GFDL shows
 199 a warm bias in most months regardless of season. CESM most closely matches the ob-
 200 servations, with only a slight warm bias.

201 E3SM shows more distinct 100 hPa temperature signals than other simulations. While
 202 still generally agreeing well with MERRA2, the E3SM model has a notable cold bias in
 203 the first decade of the simulation, after which it appears more comparable to other mod-
 204 els. This may be in part due to the different reanalysis dataset used to nudge the model:
 205 while temperature is not nudged, through the thermal wind constraint we expect the spe-
 206 cific structure of the nudged zonal winds to influence temperature. ERA-I has colder win-
 207 ter temperatures than MERRA-2 during this decade (not shown), but even compared
 208 to ERA-I temperatures, E3SM is still biased cold during this period, especially during
 209 summers. Another distinct feature of E3SM which might in part explain the increased
 210 variability in TTL temperatures is the interactive ozone scheme (Hsu and Prather (2009);
 211 Tang et al. (2011)) used in E3SM; other models use specified ozone profiles. The prog-
 212 nostic stratospheric ozone concentration in E3SM varies with local temperature, which
 213 in turn modifies temperature by changing solar heating. It is possible that such ozone
 214 feedbacks might contribute to the stronger E3SM model biases, though this was not ex-
 215 plored in detail and remains speculative.

216 While the nudging experiments are designed to ensure the meridional and zonal
 217 stratospheric winds associated with the QBO are well-captured, stratospheric biases in
 218 other variables are not necessarily constrained. In particular, nudging experiments like
 219 those reported here do not ensure that the divergent component of the circulation is strictly
 220 enforced (DeWeaver and Nigam (1997); Hitchcock and Haynes (2014); Davis et al. (2022)).

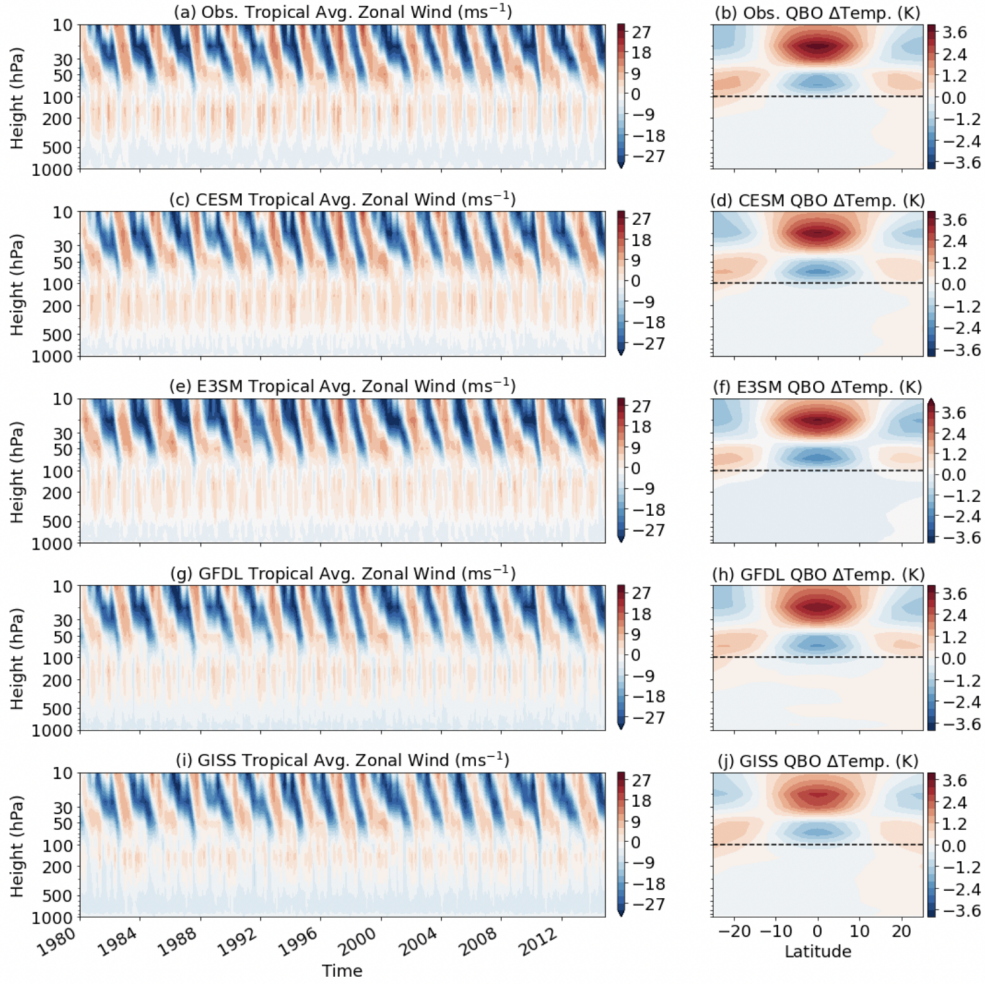


Figure 1. Left panels: The tropical mean (zonal mean averaged from 10°N-10°S) zonal wind in MERRA2 (a) and the four nudged climate simulations (c, e, g, i). Right panels: The QBOE minus QBOW zonal mean temperature in reanalysis (b) and the nudged models (d, f, h, j). The dashed black line indicates the level above which nudging is applied.

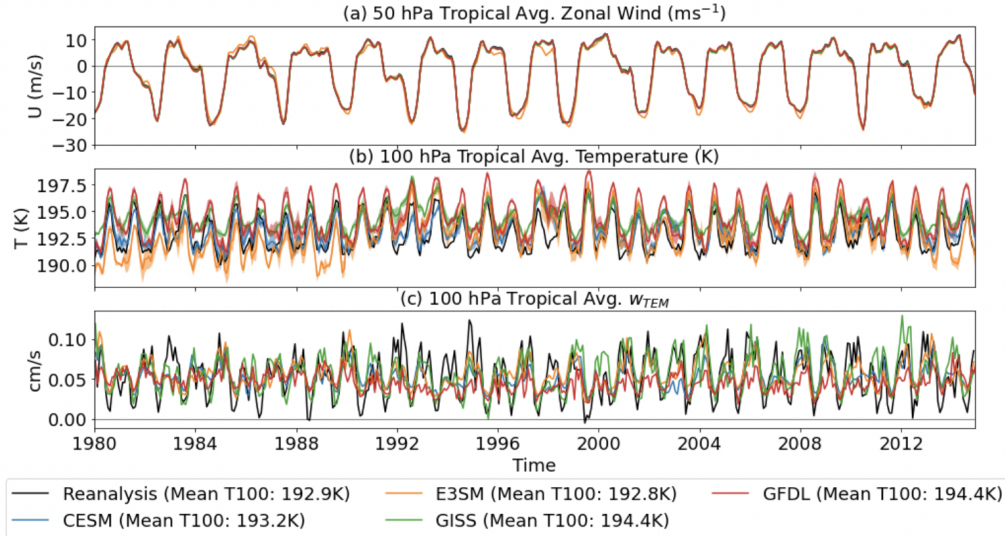


Figure 2. (a) The 10°N/S , all longitude-mean zonal wind at 50 hPa, (b) temperature at 100 hPa and (c) w_{TEM} vertical velocity at 100 hPa. Spread in shading shows the range across the ensemble of each model; shading is shown in the top panel but is essentially zero for each model. The legend indicates the model, as well as the all-time mean 100 hPa temperature (e.g. the time-mean in panel b).

221 More comprehensive (i.e. three-dimensional, full domain) nudging experiments can also
 222 exhibit large differences in the Transformed Eulerian Mean (TEM, Andrews et al. (1987))
 223 circulation compared to that of the target state, as was illustrated for models partici-
 224 pating in the Chemistry Climate Modeling Initiative (Chrysanthou et al. (2019); Orbe,
 225 Plummer, et al. (2020)). Indeed, Figure 2c, which shows time series of 100hPa residual
 226 vertical velocity (w_{TEM}) demonstrates that while there are some similarities between the
 227 reanalysis and the nudged simulations, this field is not particularly well constrained by
 228 the nudging and generally exhibits lower variability than the reanalysis, especially in the
 229 GFDL model.

230 While the TEM circulation has not been theorized as central to the QBO-MJO link,
 231 we still feel this point important to note and highlight the degree to which nudging does
 232 not constrain all aspects of the QBO-associated circulation anomalies. We highlight this
 233 issue with nudging in general, and also note this aspect of model bias as a theoretical
 234 or observational avenue that future work on the QBO-MJO link might explore.

235 3.2 MJO Representation

236 The models' tropospheres are not nudged, such that MJO performance across the
 237 four models is not constrained by observations. Nevertheless, models whose represen-
 238 tations of the MJO are reasonable were prioritized in this intercomparison, and the four
 239 models considered show MJO signals that represent relatively state-of-the-art capabil-
 240 ity in simulating the MJO (Zhao et al. (2018); Danabasoglu et al. (2020); D. Kim et al.
 241 (2022)). Figure 3 shows the observed December-February (DJF) mean OLR (Fig 3a) and
 242 standard deviation of 20-100-day bandpass-filtered, eastward wavenumber 1-5 filtered,
 243 DJF OLR (Fig 3b). The latter is often used as a metric for MJO convective activity (e.g.,
 244 Yoo and Son (2016)). Also shown are the model differences from observations (Fig 3c-
 245 j) for one ensemble member; differences in these diagnostics across ensemble members

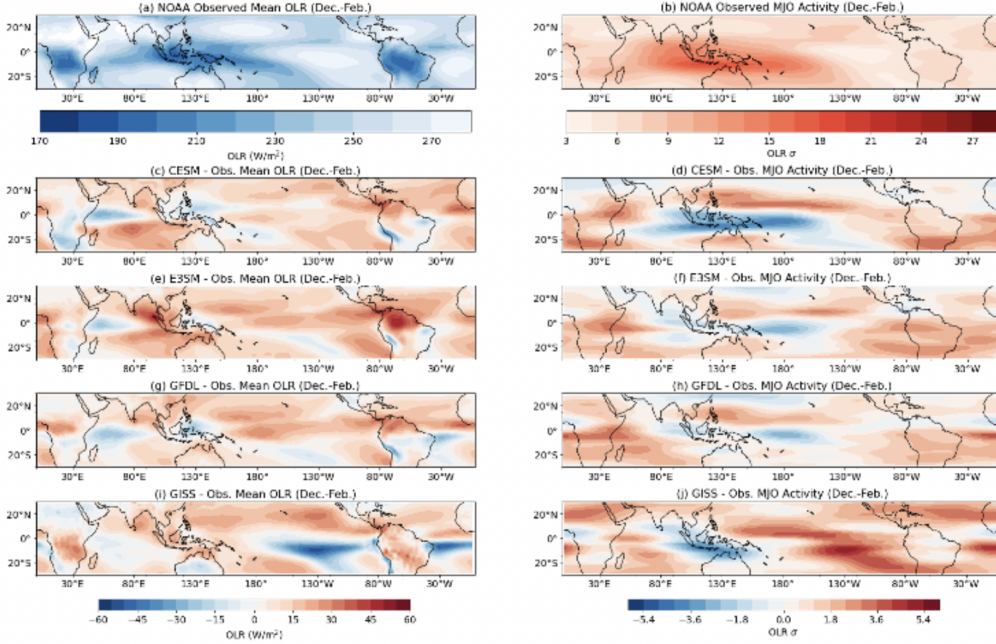


Figure 3. The observed December-February mean OLR (a) and standard deviation of 20-100 day, eastward wavenumber 1-5, bandpass-filtered OLR (b). Bottom panels (c-j) show differences between each model (interpolated onto the observed grid) and observations in both quantities.

246 are small and thus not shown. Overall, all models capture the overall distribution of winter-
 247 time convection with reasonable fidelity. A common feature in models is slightly too-low
 248 OLR over the western Indian ocean and too-strong in the subtropics. The GISS model
 249 also shows a prominent region of negative OLR bias over the eastern and central Pacific,
 250 which we hypothesize may be due to an overly active El Niño (Kelley et al. (2020)), and
 251 which is not a feature other models demonstrate.

252 Models also show biases in MJO activity, though systematic biases across all mod-
 253 els are not readily evident. Two models – CESM and GISS – show too weak MJO ac-
 254 tivity in the region of the Maritime Continent. In CESM, this is accompanied by increased
 255 winter-time MJO activity to the north of the Maritime Continent (Fig. 3d), which may
 256 indicate the MJO in this model does not detour south of the Maritime Continent to the
 257 same extent as observed. In the GISS model, stronger-than-observed MJO activity is ev-
 258 ident in the same eastern and central Pacific region where mean OLR biases are promi-
 259 nent, possibly due to an extension of convective activities east of the MJO in this model
 260 due to the increased ENSO activity. Smaller biases around the Maritime continent are
 261 evident in GFDL or E3SM; both show slightly less MJO activity, but are generally com-
 262 parable to observations.

263 Another way of measuring MJO activity and fidelity is through MJO indices – Fig-
 264 ure 4 shows several metrics of how the RMM index in the models compares with obser-
 265 vations. All models capture something akin to the observed seasonal cycle in RMM am-
 266 plitude, with higher values in boreal winter and lower values in boreal summer (Fig. 4a),
 267 though a range of seasonal cycle behavior is still evident. Models tend to overestimate
 268 MJO activity in late fall and early winter, with the GISS and CESM models looking clos-
 269 est to observations during the rest of the year. The GFDL model shows weaker ampli-
 270 tude in general during January - March, whereas E3SM shows stronger MJO amplitude
 271 during this period in particular, as well as at other points during the year. During DJF,

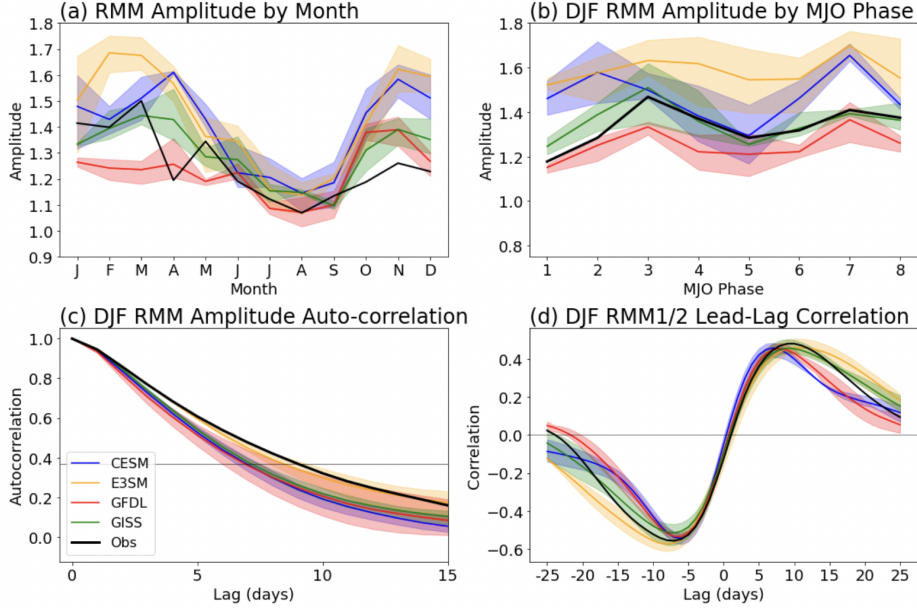


Figure 4. RMM properties for observations and each model, with shading showing the ensemble spread. Panels show (a) the RMM amplitude binned by month; (b) the RMM amplitude binned by MJO phase; (c) the lagged auto-correlation in RMM amplitude as a function of day; and (d) the lead-lag correlation between RMM1 and RMM2 as a function of day.

272 the season when the observed QBO-MJO link is evident, models show a range of RMM
 273 amplitudes. Sensitivity of RMM amplitudes to the MJO phase is not large (Fig. 4b) in
 274 models or observations, though the behavior discussed above is evident with the GFDL
 275 model having slightly weaker than observed amplitude, CESM and GISS being closer
 276 to observed, and E3SM showing stronger than observed behavior throughout all MJO
 277 phases.

278 Note this is somewhat in contrast with the weaker-than-observed signals in MJO
 279 activity in certain models, like CESM, seen in Figure 3. We attribute this difference to
 280 several aspects: MJO activity, defined in Figure 3 using bandpass-filtered OLR, measures
 281 the local subseasonal convective variability at each grid point, whereas RMM measures
 282 the global signal of the MJO across convection and circulation, with circulation signals
 283 being more dominant drivers of RMM (Ventrice et al. (2013); Straub (2013)). Biases in
 284 particular regions and variables – like convective activity over the Maritime Continent
 285 – may be offset by global wind and convective signals viewed through RMM. Composite
 286 plots of bandpass filtered OLR onto the RMM phase further confirmed that OLR signals
 287 around the Maritime Continent were weaker than observed (not shown).

288 Figure 4 also shows the lagged auto-correlation of RMM amplitude in the observations
 289 and the model, as well as the lead-lag correlation between RMM1 and RMM2.
 290 Both of these generally highlight that the models’ RMM indices compare favorably to
 291 observations, though the RMM in three models (CESM, GISS, and GFDL) has an amplitude
 292 auto-correlation that falls off faster than observed, suggesting a less persistent
 293 MJO. The lead-lag correlation is also fairly comparable, illustrating that the model MJO
 294 propagates approximately as coherently as observed. GFDL and CESM somewhat under-
 295 estimate the degree of the correlation (i.e. the minima and maxima in Figure 4d) and

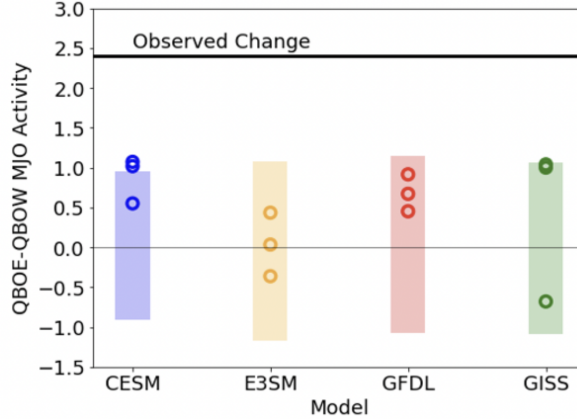


Figure 5. The change in DJF MJO activity (measured by the standard deviation (in W/m^2) of 20-100 day filtered, eastward wavenumber 1-5 OLR over the warm pool (50°E - 170°E , 20°S - 5°N), as in H. Kim et al. (2020)) between QBOE and QBOW. The thick black line indicates the observed change, while the circles for each model indicate the change in each ensemble member. The shaded bar is the 2.5–97.5 percentile range of changes in MJO activity taken across bootstrapped periods in each model when the QBO was neutral.

296 the distance between the peaks is somewhat shorter, indicating slightly faster-than-observed
 297 MJO propagation in these two models. But overall, these diagnostics confirm that MJO
 298 representation via the RMM index in models is generally comparable to observations.
 299 Some models, such as E3SM, show even stronger MJO amplitude and compare quite fa-
 300 vorably with observations.

301 3.3 The Lack of a QBO-MJO Connection

302 While QBO signals across the models are well-represented with nudging, and no
 303 clear systematic MJO bias appears via the metrics described above, none of the four mod-
 304 els shows a clear QBO-MJO connection in any ensemble member, or in the ensemble mean.
 305 We illustrate this lack of a link through both changes in the MJO activity (as defined
 306 by the 20-100 day bandpass filtered, eastward wavenumber 1-5 filtered OLR) and the
 307 correlation between the U50 and RMM indices.

308 We first examined changes in MJO activity during QBOE and QBOW winters (DJF).
 309 Figure 5 shows the difference in the standard deviation of filtered OLR over the Mar-
 310 itime continent region (50°E - 170°E , 20°S - 5°N) between QBOE and QBOW: the strong
 311 increase in the standard deviation in observations (over $2 \text{ W}/\text{m}^2$, indicating enhanced
 312 subseasonal convective variability during QBOE periods) is not evident in the models.
 313 Some ensemble members show positive changes, but none are as strong as observations,
 314 and in the GISS and E3SM models, changes of both signs are found. Note that the ob-
 315 served values in Figure 5 ($\sim 2.4 \text{ W}/\text{m}^2$) are slightly smaller than the values reported in
 316 H. Kim et al. (2020) ($\sim 2.8 \text{ W}/\text{m}^2$, see their Figure 3); further analysis (not shown) re-
 317 veals that this likely reflects our use of NOAA OLR, whereas ERAI values were used in
 318 that study. Previous studies have also noted a discrepancy in moisture variance asso-
 319 ciated with the MJO among different reanalyses (Ren et al. (2021)); more to the point,
 320 for both cases, the observed values are still significantly larger than in the models.

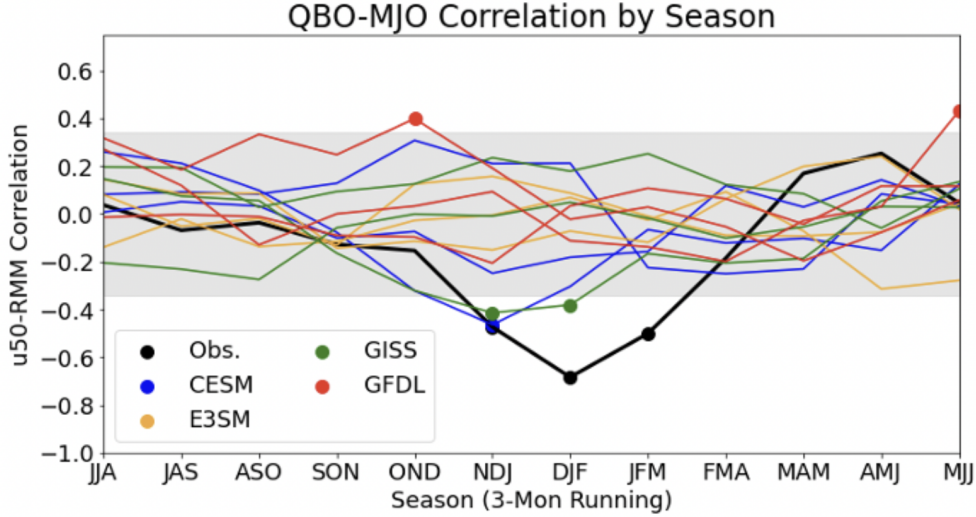


Figure 6. The correlation between the 3-month mean RMM amplitude and U50 QBO index, with the months indicated across the x-axis (beginning in June-August and ending May-July). Each ensemble member is shown separately. The grey shading denotes the 95% significance level using a t-test; correlations that are significant above or below that level are denoted with a dot.

321 Further, we conducted a bootstrap analysis to sample changes in MJO activity over
 322 randomly selected winter periods when the nudged QBO was neutral (H. Kim et al. (2020)),
 323 sampling equivalent numbers of QBOE and QBOW samples to what is found in each model.
 324 The bootstrap analysis generally produces larger or comparable magnitudes in MJO vari-
 325 ance than the models’ QBO-related signals (shaded bars in Figure 5), indicating that
 326 the simulated QBO-signals here are indistinguishable from interannual variability unas-
 327 sociated with the QBO. Two ensemble members in CESM show slightly higher change
 328 than noise, though the relationship is still half of the observed and a third ensemble mem-
 329 ber does not show the same link.

330 Analysis of the correlation between U50 and RMM in the models also does not show
 331 a strong QBO-MJO connection. While the observed QBO-MJO link is evident only in
 332 winter, we explored the correlation throughout the year across all model simulations, since
 333 an explanation for why the observed link should appear only in DJF is not forthcom-
 334 ing and a strong model link in a season aside from winter would still be of interest. Fig-
 335 ure 6 shows the correlation between 3-month mean RMM amplitude and U50 through-
 336 out the year. A dip which leads to significant anti-correlation in observations from Novem-
 337 ber-January through January-March is evident, as other studies have shown (Marshall et al.
 338 (2017); Martin, Son, et al. (2021)). Yet no model shows a seasonal modulation like that
 339 observed. One CESM and GISS ensemble member and two members of the GFDL model
 340 show limited periods of significant correlation or anticorrelation, but these are either of
 341 the wrong sign (GFDL), are over a limited period (CESM), or are much weaker than ob-
 342 served (GISS, GFDL, and CESM). As a few spurious correlations can be expected when
 343 analyzing over many ensemble members across many seasons, a few points of significance
 344 in the models are not surprising. Taken as a whole, it seems conclusive that no model
 345 shows a significant QBO-MJO link with a magnitude or characteristics comparable to
 346 that in observations. Ensemble means also show no link in any model.

347 It remains difficult to identify what explains the lack of a QBO-MJO connection
 348 in models. MJO biases, for example the 3D structure of the MJO, have been noted as
 349 a possible source of error that stratospheric nudging experiments do not resolve (M21).
 350 Yet absent a clear theoretical hypothesis for what drives the observed QBO-MJO inter-
 351 action, pin-pointing model deficiencies is a challenge. M21 explored whether aliasing be-
 352 tween the imposed QBO and different sea-surface temperature patterns showed any re-
 353 lationship to the QBO-MJO interaction, but found no clear signal.

354 Here we explore two other hypotheses recently presented in the literature (Sakaeda
 355 et al. (2020)) regarding possible metrics or mechanisms that may be important for the
 356 QBO-MJO link: cloud-radiative feedbacks and the vertical structure of the MJO. While
 357 the nudging experiments conducted here do not correct tropospheric biases in either MJO
 358 cloud feedbacks or vertical structure, diagnosing these aspects of models may illuminate
 359 any issues and help further guide hypotheses of what drives the observed QBO-MJO in-
 360 teraction and their biases in models.

361 Our first hypothesis, following Sakaeda et al. (2020), is that the uniquely strong
 362 cloud-radiative feedback associated with the observed MJO may make it especially sus-
 363 ceptible to modulation by the QBO. In particular this may explain why only the MJO
 364 and not other tropical convectively coupled waves are modulated by the QBO (Abhik
 365 and Hendon (2019); Sakaeda et al. (2020)). We note that the change in MJO cloud-radiative
 366 feedback in different QBO phases in observations does not appear statistically signifi-
 367 cant (Sakaeda et al. (2020)), making it unclear if cloud-radiative feedbacks are truly a
 368 central mechanism for the QBO-MJO link. Still, if models under-estimated the strength
 369 of MJO cloud-radiative feedbacks, it could both help explain the lack of a model QBO-
 370 MJO link and support the hypothesized importance of this physical process.

371 We diagnose MJO-related cloud-radiative feedback using the greenhouse enhance-
 372 ment parameter (D. Kim et al. (2015); Adames and Kim (2016); Sakaeda et al. (2020)),
 373 which measures how much reduction in OLR occurs due to anomalous water vapor and
 374 cloudiness per unit of precipitation. A stronger reduction in OLR indicates a colder cloud
 375 top that is generally associated with deeper convection. Our specific methodology fol-
 376 lows Adames and Kim (2016) and Sakaeda et al. (2020) by calculating the relationship
 377 between rainfall and OLR during DJF. We use 20-100 day bandpass filtered OLR and
 378 rain anomalies at latitude-longitude points from 60°E-180°E and 15°N-15°S, and due
 379 to availability of observed TRMM rainfall data, only the period 1998-2015 is used. To
 380 facilitate comparison the same time period is used in the models; model results are not
 381 sensitive to changing our analysis using all available years. Rainfall and OLR are binned
 382 every 2 W/m² for OLR and every 0.2 mm/hr for rain in Figure 7, and the slope of the
 383 regression line (“r” in Adames and Kim (2016)) represents the cloud radiative feedback
 384 parameter. The slope of this line, which is negative, indicates how strongly longwave ra-
 385 diative warming increases with rainfall.

386 Our observed value of r (-0.167) agrees very well with Adames and Kim (2016). Val-
 387 ues of r across ensemble members show that the majority of models (CESM, GFDL, GISS)
 388 show slightly weaker MJO cloud feedbacks (higher r values; listed in the top right of each
 389 panel in Figure 7), while one model (E3SM) has r values across the ensemble that cor-
 390 respond well with observations. Further, in models with weaker cloud feedbacks, biases
 391 in r relative to observations are not large compared to the observed range between the
 392 MJO and other convectively coupled equatorial waves (e.g. Sakaeda et al. (2020); their
 393 Figure 14). This shows that the models capture values of MJO cloud feedback that ap-
 394 pear only slightly weaker-than-observed, and coupled with the fact that cloud feedback
 395 in E3SM looks comparable to observations and the model has no QBO-MJO link, cap-
 396 turing the correct cloud feedback parameter is not enough to ensure a connection of the
 397 MJO to the QBO. This does not in and of itself prove cloud-radiative feedbacks are not
 398 central to the observed QBO-MJO link: more complex and subtle processes may be at
 399 play in observations, or other important processes may be missing from models. But at

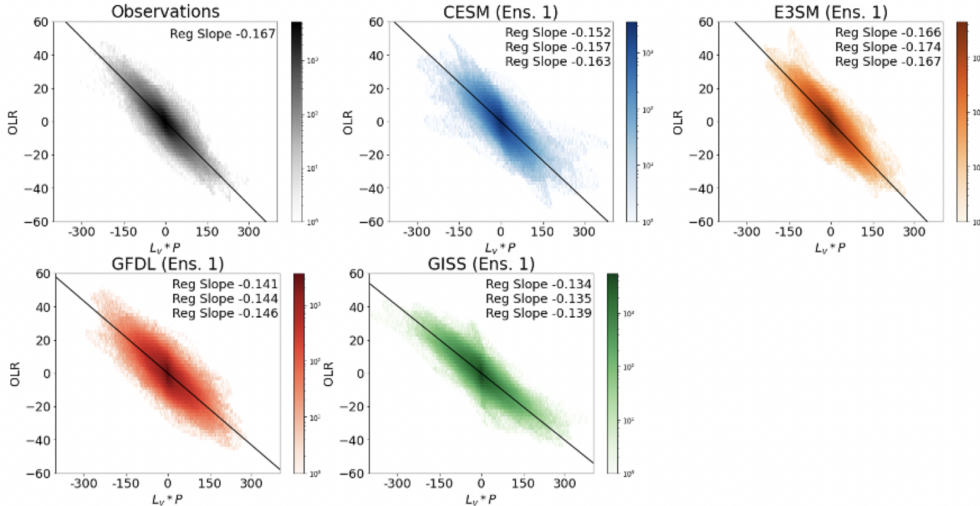


Figure 7. Shading shows the number density of 20-100 day bandpass filtered rainfall (x-axis; scaled by latent heat of vaporization) and OLR (y-axis) anomalies for 0.02 mm/hr and 2 W/m² sized bins. Panels are observations (top left) and the first ensemble member of each model (other panels). The black line is the regression coefficient between OLR and rainfall, which represents the cloud-radiative feedback parameter. The regression coefficient is listed in the top right; for the model runs, while only the first ensemble member is shown, the regression coefficient for all three members is listed.

400 least by this metric, no major deficiency is evident systematically across the model ex-
 401 periments we conducted.

402 Further analysis of how the cloud feedback parameter varied in QBOE versus QBOW
 403 across the model showed a wide range of behavior. In observations, Sakaeda et al. (2020)
 404 noted a 6% increase in r in QBOE versus QBOW; while the change was not significant,
 405 they suggested stronger cloud radiative feedbacks in QBOE may be linked to increased
 406 MJO activity in QBOE. We found no robust QBO-related change in r in model simu-
 407 lations: in all four models at least one ensemble member showed an increase of r in QBOE
 408 versus QBOW and at least one member showed a decrease, suggesting no systematic re-
 409 lationship between the imposed QBO and cloud-radiative feedbacks. The interpretation
 410 of this finding would depend on whether the observed connection between r and the QBO
 411 phase is indeed robust and at this point it's unclear whether that is the case (Sakaeda
 412 et al. (2020)). If the observed connection is robust, then the fact that the models don't
 413 exhibit it could be a potential reason for their lack of QBO-MJO connection. However,
 414 if the connection between r and the QBO is not meaningful in observations, then the model
 415 results here are consistent with there not being a true connection. Thus, future work which
 416 examines how cloud feedbacks, the QBO, and the MJO interact in observations in more
 417 detail would be very useful.

418 A second hypothesis we examine is that biases in the vertical structure of the MJO
 419 – in particular the vertical velocity – may be important. Several studies have proposed
 420 that the MJO's vertical structure may be important in explaining why and how it is mod-
 421 ulated by the QBO, either through the vertical structure of MJO temperature signals
 422 in the TTL (Hendon and Abhik 2018) or through the vertical top-heaviness of MJO ver-
 423 tical velocity (Sakaeda et al. (2020)).

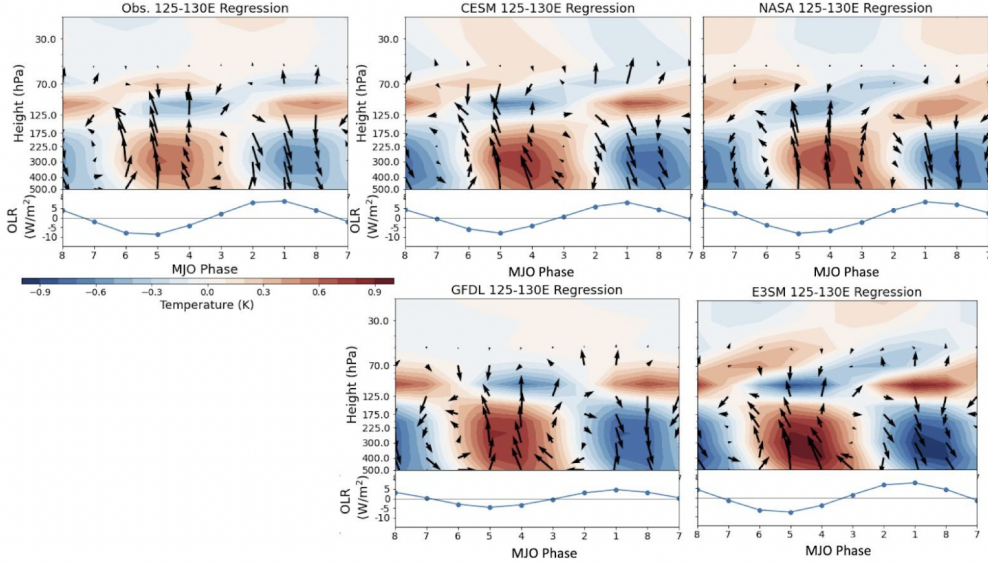


Figure 8. Regression plots of DJF temperature, zonal wind, and vertical velocity as well as OLR (bottom portion of each panel) regressed onto the RMM index. Variables are averaged from 5°S to 5°N and from 125°E to 130°E , and the seasonal cycle is removed before regressing against RMM1-RMM2 (Phase 3/4), RMM1 (Phase 4/5), RMM1 +RMM2 (Phase 5/6), and RMM2 (Phase 6/7). Multiplying these values by negative one represents MJO phases 7/8 to 2/3. The regression coefficient is scaled by the standard deviation of each variable, and vertical velocity is multiplied by -1 (upward indicates ascent), and by 1000 for ease of interpretation. The y-axis is log pressure.

424 We diagnose how well the models represent the MJO’s vertical structure via a re-
 425 gression analysis focusing in particular on equatorial signals in vertical velocity, zonal
 426 wind, and temperature around the Maritime Continent region where the observed QBO-
 427 MJO link is strongest (Fig. 3b). Figure 8 shows wind and temperature signals around
 428 the Maritime Continent regressed onto RMM phases 1-8 following the methodology de-
 429 scribed in Hendon and Abhik (2018) for ERA-5 reanalysis and the four models. Mod-
 430 els show a range of vertical structures in temperature and wind that look generally quite
 431 similar to the observations (Figure 8). In particular, all models show TTL “cold caps”
 432 (Holloway and Neelin (2007)) above and slightly east of peak convection in MJO phases
 433 4 and 5. The precise phasing and magnitude of model cold caps differ somewhat: the
 434 signal is slightly too weak in the GISS model (as noted in M21), but has comparable strength
 435 to reanalysis in the other three models. Most models also show upward propagation of
 436 Kelvin waves into the stratosphere emanating from the MJO (upward tilting warm and
 437 cold anomalies above ~ 125 hPa), though this feature is not evident in the GFDL model.

438 While temperature and wind signals look comparable in Figure 8, we examined the
 439 model MJO vertical velocity in more detail, as Sakaeda et al. (2020) have pointed to the
 440 top-heaviness of MJO vertical velocity as possibly important for the observed QBO-MJO
 441 link. Again we focus on vertical velocity signals around the Maritime Continent where
 442 the observed QBO-MJO link is strongest. Figure 9 shows a similar regression plot to Fig-
 443 ure 8, regressing vertical velocity against RMM1 (corresponding to the MJO phase 4/5)
 444 and taking a slightly broader 120°E - 150°E region where strong convection during active
 445 MJO is evident. Comparison of reanalysis and model vertical velocity (Figure 9) indi-

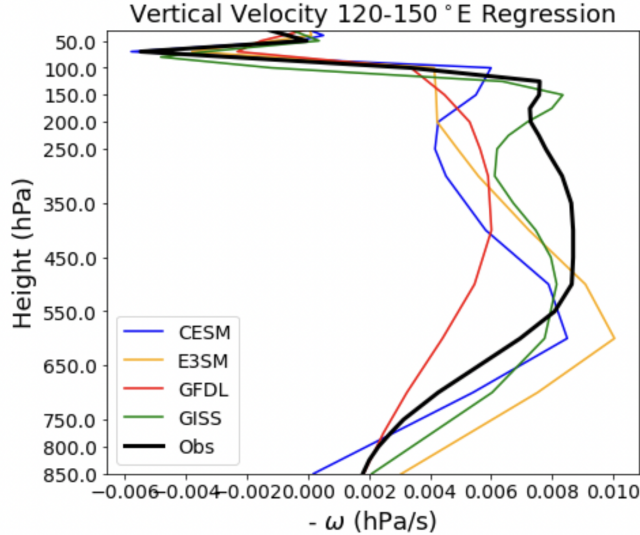


Figure 9. Regression plots of DJF vertical velocity, similar to Figure 8, but for MJO phase 4/5 (e.g., regression onto RMM 1) averaged over 120°E-150°E (e.g. capturing active MJO conditions over the Maritime Continent, and averaging over the region of deep convection and ascent).

446 cates that models tend to show vertical velocity profiles associated with the MJO around
 447 the MC that are either too bottom-heavy (E3SM, CESM, NASA), or too weak overall
 448 (GFDL). For bottom-heavy models, vertical velocity peaks in the upper troposphere around
 449 600 hPa, whereas the observed peak tends to be between 400-500 hPa, consistent qual-
 450 itatively with other studies (Inoue et al. (2020); Sakaeda et al. (2020)). In the case of
 451 the GFDL model, the peak in vertical velocity is more comparable to the reanalysis but
 452 overall ascent is much weaker throughout the troposphere (although we caution that the
 453 reanalysis vertical velocity probably has an important contribution from underlying model
 454 physics as well).

455 This points to a potential common deficiency across models related to the verti-
 456 cal structure of the vertical velocity. Coupled with a weaker cloud-radiative feedback in
 457 some models, it is possible that this may in part contribute to the lack of a QBO-MJO
 458 link observed, though we note that E3SM shows a comparable cloud-radiative feedback
 459 to that observed and still did not possess a QBO-MJO link. This makes it difficult to
 460 point directly to biases in vertical velocity as the main culprit of the missing QBO-MJO
 461 link in models, but does suggest more work centered on understanding how vertical ve-
 462 locity profiles associated with MJO convection, and more generally the vertical struc-
 463 ture of the MJO, may be connected to the QBO-MJO linkage would be valuable and pos-
 464 sibly illuminating.

465 **4 Discussion and Conclusions**

466 The observed QBO-MJO connection – an increase in MJO activity in the easterly
 467 phase of QBO relative to the westerly phase – remains difficult to capture in free-running
 468 climate models. Building on previous work (M21), we carried out a series of experiments
 469 in which the stratosphere in four climate models was nudged towards reanalysis, impos-
 470 ing QBO signals while allowing the troposphere to freely evolve. The four state-of-the-
 471 art climate models were run from 1980-2015, with three ensemble members per simu-
 472 lation, nudged towards reanalysis during that period. Despite very good representation

473 of the key aspects of the QBO, including wind and temperature signals, we find no that
474 no model exhibits a QBO-MJO connection that is comparable to that in observations.

475 In examining the possible cause of why models show no QBO-MJO link, we explored
476 model representation of the MJO, including the vertical structure of the MJO around
477 the Maritime Continent, and cloud-radiative feedbacks associated with the observed ver-
478 sus modeled MJO. Too-weak cloud-radiative feedbacks were one hypothesized reason for
479 the lack of the QBO-MJO link, but that does not appear to be the case overall: MJO-
480 related cloud-radiative feedbacks were somewhat weaker than observed in most models,
481 but one (E3SM) showed values consistent with observations and still failed to show a QBO-
482 MJO link. This does not mean that clouds are not central to the observed link, but high-
483 lights the need for more specific and testable hypotheses. In particular, we noted that
484 while the observed MJO cloud-radiative feedbacks strengthened slightly during QBOE,
485 models do not simulate this change. Whether this indicates that the observed change
486 is not significant (as was found in Sakaeda et al. (2020)) or that the models miss an im-
487 portant process remains unresolved.

488 We showed that models have vertical structures of wind and temperature that are
489 largely consistent with observations, including finding that all models represent a cold
490 cap above active MJO convection. However, model vertical velocity appears either weaker
491 or more bottom-heavy than observed. Sakaeda et al. (2020) identified the top-heavy na-
492 ture of MJO vertical velocity as possibly important for explaining features of the observed
493 QBO-MJO connection, like why it manifests only in winter, while other convectively cou-
494 pled waves are not affected (Abhik and Hendon (2019); Sakaeda et al. (2020)), and why
495 an observed QBO-MJO link does not appear to have existed prior to ~ 1980 (Klotzbach
496 et al. (2019)). A specific hypothesis regarding how the MJO's vertical structure may link
497 the QBO and MJO is still lacking however, and future work examining this aspect of the
498 QBO-MJO link may also be fruitful.

499 Overall, however, it remains possible that a host of other model biases or processes
500 could contribute to the lack of a QBO-MJO connection. The results here, coupled with
501 findings in M21 using a larger ensemble in a single model, strongly suggest that nudg-
502 ing of the QBO winds in conventional climate models is not sufficient to capture a QBO-
503 MJO connection. This implies that stratospheric biases in the zonal wind or the tem-
504 perature of the tropics of climate models is not the reason, or at least not the only rea-
505 son, why models fail to simulate the QBO-MJO connection. Stratospheric biases still ex-
506 ist with nudging however; as we noted, the divergent TEM circulation in the stratosphere
507 for example is much less constrained with nudging. It is not clear whether this is impor-
508 tant for the QBO-MJO link, but continuing to examine other stratospheric biases in mod-
509 els as they relate to the MJO may help guide future modeling strategies. Further, tro-
510 pospheric biases may be important, especially as they relate to the MJO, or having an
511 interactive stratosphere rather than a nudged one may be central for capturing the QBO-
512 MJO connection through improved representation of the QBO descent into the lower-
513 most stratosphere (Butchart et al. (2003); DallaSanta et al. (2021)), while also not lim-
514 iting wave-mean flow interactions. We recommend future approaches or modeling ex-
515 periments in particular to look at different modeling frameworks, perhaps at higher res-
516 olution using super-parameterization.

517 Finally, we emphasize that the dataset here offers a unique suite of experiments in
518 which to examine other questions related to downward stratospheric impacts in climate
519 models, not limited to those in the tropics. Future work leveraging the output from these
520 model experiments may therefore be of interest to the broader stratosphere-troposphere
521 community.

Open Research Section

All observational and reanalysis datasets used in this study are publicly available. The RMM index is available at <http://www.bom.gov.au/climate/mjo/graphics/rmm.74toRealtime.txt>. For reanalysis and observed data, NOAA Interpolated OLR (Liebmann and Smith (1996)) is available at https://psl.noaa.gov/data/gridded/data.interp_OLR.html; ERA-5 reanalysis (Hersbach et al. (2020)) is available at <https://cds.climate.copernicus.eu/#!/search?text=ERA5&type=dataset>. TRMM data is available from https://disc.gsfc.nasa.gov/datasets/TRMM_3B42_Daily_7/summary.

Data from the modeling experiments used in the figure and analysis in this study is presently available from the first-author, but during the review process will be uploaded to an open access data repository (e.g. Zenodo) and made freely available there.

Acknowledgments

ZM acknowledges support from the National Science Foundation under Award No. 2020305. This work was supported by the National Center for Atmospheric Research, which is a major facility sponsored by the National Science Foundation (NSF) under Cooperative Agreement No. 1852977. The CESM simulations were run with NCAR Community Computing on the Computational and Information Systems Laboratory's Cheyenne system (doi:10.5065/D6RX99HX). Portions of this study were supported by the Regional and Global Model Analysis (RGMA) component of the Earth and Environmental System Modeling Program of the U.S. Department of Energy's Office of Biological Environmental Research (BER) via National Science Foundation IA 1947282, and under Award Number DE-SC0022070. The E3SM simulations were supported by the Energy Exascale Earth System Model (E3SM) project, funded by the DOE BER through the Earth System Model Development program area using computing resources provided by the National Energy Research Scientific Computing Center (NERSC), a DOE Office of Science User Facility supported by the Office of Science of DOE under contract DE-AC02-05CH11231. The Pacific Northwest National Laboratory (PNNL) is operated for DOE by Battelle Memorial Institute under contract DE-AC05-76RL01830. Work at (Lawrence Livermore National Laboratory) LLNL was performed under the auspices of the U. S. DOE by LLNL under contract No. DE-AC52-07NA27344. Support has also been received from the LLNL LDRD project 22-ERD-008, "Multiscale Wildfire Simulation Framework and Remote Sensing". P. Lin is supported under award NA18OAR4320123 from the National Oceanic and Atmospheric Administration, U.S. Department of Commerce. The statements, findings, conclusions, and recommendations are those of the author(s) and do not necessarily reflect the views of the National Oceanic and Atmospheric Administration, or the U.S. Department of Commerce. We acknowledge GFDL resources made available for this research. Climate modeling at GISS is supported by the NASA Modeling, Analysis and Prediction program, and resources supporting this work were provided by the NASA High-End Computing (HEC) Program through the NASA Center for Climate Simulation (NCCS) at Goddard Space Flight Center. H. Kim was supported by the NSF grant AGS-1652289 and Korean Meteorological Administration (KMA) RD Program Grant KMI2021-01210.

References

- Abhik, S., & Hendon, H. H. (2019). Influence of the qbo on the mjo during coupled model multiweek forecasts. *Geophysical Research Letters*, *46*(15), 9213–9221.
- Adames, Á. F., & Kim, D. (2016). The mjo as a dispersive, convectively coupled moisture wave: Theory and observations. *Journal of the Atmospheric Sciences*, *73*(3), 913–941.
- Ahn, M.-S., Kim, D., Kang, D., Lee, J., Sperber, K. R., Gleckler, P. J., ... Kim,

- 571 H. (2020). Mjo propagation across the maritime continent: Are cmip6
572 models better than cmip5 models? *Geophysical Research Letters*, *47*(11),
573 e2020GL087250.
- 574 Andrews, D. G., Holton, J. R., & Leovy, C. B. (1987). *Middle atmosphere dynamics*
575 (No. 40). Academic press.
- 576 Anstey, J. A., Simpson, I. R., Richter, J. H., Naoe, H., Taguchi, M., Serva, F., ...
577 others (2022). Teleconnections of the quasi-biennial oscillation in a multi-
578 model ensemble of qbo-resolving models. *Quarterly Journal of the Royal*
579 *Meteorological Society*, *148*(744), 1568–1592.
- 580 Back, S.-Y., Han, J.-Y., & Son, S.-W. (2020). Modeling evidence of qbo-mjo connec-
581 tion: A case study. *Geophysical Research Letters*, *47*(20), e2020GL089480.
- 582 Baldwin, M., Gray, L., Dunkerton, T., Hamilton, K., Haynes, P., Randel, W. J., ...
583 others (2001). The quasi-biennial oscillation. *Reviews of Geophysics*, *39*(2),
584 179–229.
- 585 Butchart, N., Scaife, A. A., Austin, J., Hare, S. H., & Knight, J. R. (2003). Quasi-
586 biennial oscillation in ozone in a coupled chemistry-climate model. *Journal of*
587 *Geophysical Research: Atmospheres*, *108*(D15).
- 588 Camargo, S. J., & Sobel, A. H. (2010). Revisiting the influence of the quasi-biennial
589 oscillation on tropical cyclone activity. *Journal of Climate*, *23*(21), 5810–5825.
- 590 Chrysanthou, A., Maycock, A. C., Chipperfield, M. P., Dhomse, S., Garny, H.,
591 Kinnison, D., ... others (2019). The effect of atmospheric nudging on the
592 stratospheric residual circulation in chemistry–climate models. *Atmospheric*
593 *Chemistry and Physics*, *19*(17), 11559–11586.
- 594 DallaSanta, K., Orbe, C., Rind, D., Nazarenko, L., & Jonas, J. (2021). Dynamical
595 and trace gas responses of the quasi-biennial oscillation to increased co2. *Jour-*
596 *nal of Geophysical Research: Atmospheres*, *126*(6), e2020JD034151.
- 597 Danabasoglu, G., Lamarque, J.-F., Bacmeister, J., Bailey, D., DuVivier, A., Ed-
598 wards, J., ... others (2020). The community earth system model ver-
599 sion 2 (cesm2). *Journal of Advances in Modeling Earth Systems*, *12*(2),
600 e2019MS001916.
- 601 Davis, N. A., Callaghan, P., Simpson, I. R., & Tilmes, S. (2022). Specified dynamics
602 scheme impacts on wave-mean flow dynamics, convection, and tracer transport
603 in cesm2 (waccm6). *Atmospheric Chemistry and Physics*, *22*(1), 197–214.
- 604 Dee, D. P., Uppala, S. M., Simmons, A. J., Berrisford, P., Poli, P., Kobayashi, S.,
605 ... others (2011). The era-interim reanalysis: Configuration and performance
606 of the data assimilation system. *Quarterly Journal of the royal meteorological*
607 *society*, *137*(656), 553–597.
- 608 DeWeaver, E., & Nigam, S. (1997). Dynamics of zonal-mean flow assimilation and
609 implications for winter circulation anomalies. *Journal of the atmospheric sci-*
610 *ences*, *54*(13), 1758–1775.
- 611 Douville, H. (2009). Stratospheric polar vortex influence on northern hemisphere
612 winter climate variability. *Geophysical Research Letters*, *36*(18).
- 613 Ebdon, R. (1960). Notes on the wind flow at 50 mb in tropical and sub-tropical re-
614 gions in january 1957 and january 1958. *Quarterly Journal of the Royal Meteo-*
615 *rological Society*, *86*(370), 540–542.
- 616 Eyring, V., Bony, S., Meehl, G. A., Senior, C. A., Stevens, B., Stouffer, R. J., &
617 Taylor, K. E. (2016). Overview of the coupled model intercomparison project
618 phase 6 (cmip6) experimental design and organization. *Geoscientific Model*
619 *Development*, *9*(5), 1937–1958.
- 620 Feng, P.-N., & Lin, H. (2019). Modulation of the mjo-related teleconnections by the
621 qbo. *Journal of Geophysical Research: Atmospheres*, *124*(22), 12022–12033.
- 622 Ferranti, L., Palmer, T., Molteni, F., & Klinker, E. (1990). Tropical-extratropical
623 interaction associated with the 30–60 day oscillation and its impact on medium
624 and extended range prediction. *Journal of the Atmospheric Sciences*, *47*(18),
625 2177–2199.

- 626 Garfinkel, C. I., & Hartmann, D. L. (2011). The influence of the quasi-biennial oscil-
 627 lation on the troposphere in winter in a hierarchy of models. part ii: Perpetual
 628 winter waccm runs. *Journal of the Atmospheric Sciences*, *68*(9), 2026–2041.
- 629 Gelaro, R., McCarty, W., Suárez, M. J., Todling, R., Molod, A., Takacs, L., ...
 630 others (2017). The modern-era retrospective analysis for research and applica-
 631 tions, version 2 (merra-2). *Journal of climate*, *30*(14), 5419–5454.
- 632 Gerber, E. P., & Manzini, E. (2016). The dynamics and variability model intercom-
 633 parison project (dynvarmip) for cmip6: assessing the stratosphere–troposphere
 634 system. *Geoscientific Model Development*, *9*(9), 3413–3425.
- 635 Golaz, J.-C., Caldwell, P. M., Van Roekel, L. P., Petersen, M. R., Tang, Q., Wolfe,
 636 J. D., ... others (2019). The doe e3sm coupled model version 1: Overview
 637 and evaluation at standard resolution. *Journal of Advances in Modeling Earth*
 638 *Systems*, *11*(7), 2089–2129.
- 639 Gray, L. J., Anstey, J. A., Kawatani, Y., Lu, H., Osprey, S., & Schenzinger, V.
 640 (2018). Surface impacts of the quasi biennial oscillation. *Atmospheric Chem-*
 641 *istry and Physics*, *18*(11), 8227–8247.
- 642 Held, I., Guo, H., Adcroft, A., Dunne, J., Horowitz, L., Krasting, J., ... others
 643 (2019). Structure and performance of gfdl’s cm4. 0 climate model. *Journal of*
 644 *Advances in Modeling Earth Systems*, *11*(11), 3691–3727.
- 645 Hendon, H. H., & Abhik, S. (2018). Differences in vertical structure of the madden-
 646 julian oscillation associated with the quasi-biennial oscillation. *Geophysical Re-*
 647 *search Letters*, *45*(9), 4419–4428.
- 648 Hersbach, H., Bell, B., Berrisford, P., Hirahara, S., Horányi, A., Muñoz-Sabater, J.,
 649 ... others (2020). The era5 global reanalysis. *Quarterly Journal of the Royal*
 650 *Meteorological Society*, *146*(730), 1999–2049.
- 651 Hitchcock, P., & Haynes, P. H. (2014). Zonally symmetric adjustment in the pres-
 652 ence of artificial relaxation. *Journal of the Atmospheric Sciences*, *71*(11),
 653 4349–4368.
- 654 Hitchcock, P., & Simpson, I. R. (2014). The downward influence of stratospheric
 655 sudden warmings. *Journal of the Atmospheric Sciences*, *71*(10), 3856–3876.
- 656 Holloway, C. E., & Neelin, J. D. (2007). The convective cold top and quasi equilib-
 657 rium. *Journal of the atmospheric sciences*, *64*(5), 1467–1487.
- 658 Holton, J. R., & Tan, H.-C. (1980). The influence of the equatorial quasi-biennial os-
 659 cillation on the global circulation at 50 mb. *Journal of Atmospheric Sciences*,
 660 *37*(10), 2200–2208.
- 661 Hsu, J., & Prather, M. J. (2009). Stratospheric variability and tropospheric ozone.
 662 *Journal of Geophysical Research: Atmospheres*, *114*(D6).
- 663 Inoue, K., Adames, Á. F., & Yasunaga, K. (2020). Vertical velocity profiles in con-
 664 vectively coupled equatorial waves and mjo: New diagnoses of vertical velocity
 665 profiles in the wavenumber–frequency domain. *Journal of the Atmospheric*
 666 *Sciences*, *77*(6), 2139–2162.
- 667 Jeuken, A., Siegmund, P., Heijboer, L., Feichter, J., & Bengtsson, L. (1996). On
 668 the potential of assimilating meteorological analyses in a global climate model
 669 for the purpose of model validation. *Journal of Geophysical Research: Atmo-*
 670 *spheres*, *101*(D12), 16939–16950.
- 671 Kelley, M., Schmidt, G. A., Nazarenko, L. S., Bauer, S. E., Ruedy, R., Russell,
 672 G. L., ... others (2020). Giss-e2. 1: Configurations and climatology. *Journal*
 673 *of Advances in Modeling Earth Systems*, *12*(8), e2019MS002025.
- 674 Kiladis, G. N., Dias, J., Straub, K. H., Wheeler, M. C., Tulich, S. N., Kikuchi, K.,
 675 ... Ventrice, M. J. (2014). A comparison of olr and circulation-based indices
 676 for tracking the mjo. *Monthly Weather Review*, *142*(5), 1697–1715.
- 677 Kim, D., Ahn, M.-S., Kang, I.-S., & Del Genio, A. D. (2015). Role of longwave
 678 cloud–radiation feedback in the simulation of the madden–julian oscillation.
 679 *Journal of Climate*, *28*(17), 6979–6994.
- 680 Kim, D., Kang, D., Ahn, M.-S., DeMott, C., Hsu, C.-W., Yoo, C., ... Rasch, P. J.

- 681 (2022). The madden–julian oscillation in the energy exascale earth system
682 model version 1. *Journal of Advances in Modeling Earth Systems*, 14(2),
683 e2021MS002842.
- 684 Kim, H., Caron, J. M., Richter, J. H., & Simpson, I. R. (2020). The lack of qbo-
685 mjo connection in cmip6 models. *Geophysical Research Letters*, 47(11),
686 e2020GL087295.
- 687 Kim, H., Richter, J. H., & Martin, Z. (2019). Insignificant qbo-mjo prediction skill
688 relationship in the subx and s2s subseasonal reforecasts. *Journal of Geophysi-
689 cal Research: Atmospheres*, 124(23), 12655–12666.
- 690 Klotzbach, P., Abhik, S., Hendon, H., Bell, M., Lucas, C., G. Marshall, A., & Oliver,
691 E. (2019). On the emerging relationship between the stratospheric quasi-
692 biennial oscillation and the madden–julian oscillation. *Scientific reports*, 9(1),
693 2981.
- 694 Lee, J. C., & Klingaman, N. P. (2018). The effect of the quasi-biennial oscillation
695 on the madden–julian oscillation in the met office unified model global ocean
696 mixed layer configuration. *Atmospheric Science Letters*, 19(5), e816.
- 697 Liebmann, B., & Smith, C. A. (1996). Description of a complete (interpolated) out-
698 going longwave radiation dataset. *Bulletin of the American Meteorological So-
699 ciety*, 77(6), 1275–1277.
- 700 Lim, Y., & Son, S.-W. (2020). Qbo-mjo connection in cmip5 models. *Journal of
701 Geophysical Research: Atmospheres*, 125(12), e2019JD032157.
- 702 Lim, Y., Son, S.-W., Marshall, A. G., Hendon, H. H., & Seo, K.-H. (2019). Influence
703 of the qbo on mjo prediction skill in the subseasonal-to-seasonal prediction
704 models. *Climate Dynamics*, 53, 1681–1695.
- 705 Liu, Z., Ostrenga, D., Teng, W., & Kempler, S. (2012). Tropical rainfall measuring
706 mission (trmm) precipitation data and services for research and applications.
707 *Bulletin of the American Meteorological Society*, 93(9), 1317–1325.
- 708 Madden, R. A., & Julian, P. R. (1971). Detection of a 40–50 day oscillation in
709 the zonal wind in the tropical pacific. *Journal of Atmospheric Sciences*, 28(5),
710 702–708.
- 711 Madden, R. A., & Julian, P. R. (1972). Description of global-scale circulation cells
712 in the tropics with a 40–50 day period. *Journal of Atmospheric Sciences*,
713 29(6), 1109–1123.
- 714 Marshall, A. G., Hendon, H. H., Son, S.-W., & Lim, Y. (2017). Impact of the quasi-
715 biennial oscillation on predictability of the madden–julian oscillation. *Climate
716 Dynamics*, 49, 1365–1377.
- 717 Martin, Z., Orbe, C., Wang, S., & Sobel, A. (2021). The mjo–qbo relationship in a
718 gcm with stratospheric nudging. *Journal of Climate*, 34(11), 4603–4624.
- 719 Martin, Z., Son, S.-W., Butler, A., Hendon, H., Kim, H., Sobel, A., . . . Zhang, C.
720 (2021). The influence of the quasi-biennial oscillation on the madden–julian
721 oscillation. *Nature Reviews Earth & Environment*, 2(7), 477–489.
- 722 Martin, Z., Vitart, F., Wang, S., & Sobel, A. (2020). The impact of the stratosphere
723 on the mjo in a forecast model. *Journal of Geophysical Research: Atmospheres*,
724 125(4), e2019JD032106.
- 725 Martin, Z., Wang, S., Nie, J., & Sobel, A. (2019). The impact of the qbo on mjo
726 convection in cloud-resolving simulations. *Journal of the Atmospheric Sci-
727 ences*, 76(3), 669–688.
- 728 Mayer, K. J., & Barnes, E. A. (2020). Subseasonal midlatitude prediction skill
729 following quasi-biennial oscillation and madden–julian oscillation activity.
730 *Weather and Climate Dynamics*, 1(1), 247–259.
- 731 Orbe, C., Plummer, D. A., Waugh, D. W., Yang, H., Jöckel, P., Kinnison, D. E., . . .
732 others (2020). Description and evaluation of the specified-dynamics experi-
733 ment? $\text{\textbackslash}break?i$ in the chemistry-climate model initiative. *Atmospheric
734 Chemistry and Physics*, 20(6), 3809–3840.
- 735 Orbe, C., Van Roekel, L., Adames, Á. F., Dezfuli, A., Fasullo, J., Gleckler, P. J., . . .

- 736 others (2020). Representation of modes of variability in six us climate models.
 737 *Journal of Climate*, *33*(17), 7591–7617.
- 738 Reed, R. J., Campbell, W. J., Rasmussen, L. A., & Rogers, D. G. (1961). Evidence
 739 of a downward-propagating, annual wind reversal in the equatorial strato-
 740 sphere. *Journal of Geophysical Research*, *66*(3), 813–818.
- 741 Ren, P., Kim, D., Ahn, M.-S., Kang, D., & Ren, H.-L. (2021). Intercomparison of
 742 mjo column moist static energy and water vapor budget among six modern
 743 reanalysis products. *Journal of Climate*, *34*(8), 2977–3001.
- 744 Richter, J. H., Anstey, J. A., Butchart, N., Kawatani, Y., Meehl, G. A., Osprey, S.,
 745 & Simpson, I. R. (2020). Progress in simulating the quasi-biennial oscillation
 746 in cmip models. *Journal of Geophysical Research: Atmospheres*, *125*(8),
 747 e2019JD032362.
- 748 Sakaeda, N., Dias, J., & Kiladis, G. N. (2020). The unique characteristics and poten-
 749 tial mechanisms of the mjo-qbo relationship. *Journal of Geophysical Research:*
 750 *Atmospheres*, *125*(17), e2020JD033196.
- 751 Simpson, I., Hitchcock, P., Shepherd, T., & Scinocca, J. (2011). Stratospheric vari-
 752 ability and tropospheric annular-mode timescales. *Geophysical Research Let-*
 753 *ters*, *38*(20).
- 754 Son, S.-W., Lim, Y., Yoo, C., Hendon, H. H., & Kim, J. (2017). Stratospheric control
 755 of the madden–julian oscillation. *Journal of Climate*, *30*(6), 1909–1922.
- 756 Straub, K. H. (2013). Mjo initiation in the real-time multivariate mjo index. *Journal*
 757 *of Climate*, *26*(4), 1130–1151.
- 758 Tang, Q., Prather, M., & Hsu, J. (2011). Stratosphere-troposphere exchange ozone
 759 flux related to deep convection. *Geophysical Research Letters*, *38*(3).
- 760 Toms, B. A., Barnes, E. A., Maloney, E. D., & van den Heever, S. C. (2020). The
 761 global teleconnection signature of the madden–julian oscillation and its mod-
 762 ulation by the quasi-biennial oscillation. *Journal of Geophysical Research:*
 763 *Atmospheres*, *125*(7), e2020JD032653.
- 764 Ventrice, M. J., Wheeler, M. C., Hendon, H. H., Schreck, C. J., Thorncroft, C. D., &
 765 Kiladis, G. N. (2013). A modified multivariate madden–julian oscillation index
 766 using velocity potential. *Monthly Weather Review*, *141*(12), 4197–4210.
- 767 Wang, J., Kim, H.-M., Chang, E. K., & Son, S.-W. (2018). Modulation of the mjo
 768 and north pacific storm track relationship by the qbo. *Journal of Geophysical*
 769 *Research: Atmospheres*, *123*(8), 3976–3992.
- 770 Wang, S., Tippett, M. K., Sobel, A. H., Martin, Z. K., & Vitart, F. (2019). Im-
 771 pact of the qbo on prediction and predictability of the mjo convection. *Journal*
 772 *of Geophysical Research: Atmospheres*, *124*(22), 11766–11782.
- 773 Wheeler, M. C., & Hendon, H. H. (2004). An all-season real-time multivariate
 774 mjo index: Development of an index for monitoring and prediction. *Monthly*
 775 *weather review*, *132*(8), 1917–1932.
- 776 Yoo, C., & Son, S.-W. (2016). Modulation of the boreal wintertime madden–julian
 777 oscillation by the stratospheric quasi-biennial oscillation. *Geophysical Research*
 778 *Letters*, *43*(3), 1392–1398.
- 779 Zhao, M., Golaz, J.-C., Held, I., Guo, H., Balaji, V., Benson, R., . . . others (2018).
 780 The gfdl global atmosphere and land model am4. 0/lm4. 0: 1. simulation
 781 characteristics with prescribed ssts. *Journal of Advances in Modeling Earth*
 782 *Systems*, *10*(3), 691–734.